

Properties of the electronic density of states in TiO₂ nanoparticles surrounded with aqueous electrolyte

Ilana Abayev · Arie Zaban · Vladimir G. Kytin ·
Alexey A. Danilin · Germà Garcia-Belmonte ·
Juan Bisquert

Received: 11 June 2006 / Revised: 28 August 2006 / Accepted: 4 September 2006 / Published online: 4 November 2006
© Springer-Verlag 2006

Abstract Results on the density of states of nanostructured TiO₂ as a function of particle size and temperature are reported. In TiO₂ nanoparticles with a mean diameter 10 nm, the density of states (DOS) is strongly temperature-dependent, indicating a rearrangement of the bandgap states in which the exponential energy parameter (width of the distribution) increases from 0.080 to 50 °C. For nanoparticles with mean diameters of 20 and 30 nm the DOS is much closer to an exponential distribution, and is much less sensitive to temperature variations. It is suggested that nanometer confinement has a significant influence on the density of electronic states for 10-nm particles, while band tailing is similar to that occurring in bulk semiconductors for the larger particles.

Introduction

Nanostructured metal oxide films formed by an assembly of nanoparticles sintered over a conducting substrate provide a large internal area that can realize different functionalities. In particular, nanostructured TiO₂ has received intense attention in view of the application in several types of devices, such as sensors [1], electrochromic windows [2],

electrical paint displays [3], and dye-sensitized solar cells [4]. Because all of these applications involve electron transport in the semiconductor network and interfacial charge transfer at the nanoparticles surface, it is extremely important to understand in detail the distribution and the nature of the electronic states in the semiconductor. The characteristic size of the nanoparticles used in the aforementioned applications is in the range of 10–40 nm. The density of states (DOS) should be strongly influenced by the large surface to volume ratio of the nanoparticles, and the presence of surrounding media such as liquid or solid electrolyte.

The DOS in nanostructured TiO₂ was investigated using a variety of methods: cyclic voltammetry (CV) [5], impedance spectroscopy [6], voltage decay charge extraction method [7, 8], and potential step-current integration (chronoamperometry) [9, 10]. These methods are based on the determination of the chemical capacitance [11], i.e., of the change of the number of electrons in the film, n , under a small variation of the Fermi level, E_{Fn} , by controlling the potential in the film $U = -(E_{Fn} - E_{F0})/q$, where q denotes elementary charge and E_{F0} the electron Fermi level in TiO₂ in the absence of bias potential, which equals the redox potential in the electrolyte, $E_{F,redox}$. Most previous reports [5, 7–9] agree in the existence of an exponential distribution of bandgap states in nanostructured TiO₂ of the form

$$g(E) = \frac{N_L}{k_B \cdot T_0} \exp [(E - E_c)/(k_B \cdot T_0)] \quad (1)$$

Here, k_B is Boltzmann's constant, E is the energy that decreases downward in the bandgap, E_c is the energy of the lower edge of the conduction band, N_L is the total DOS, and T_0 is a parameter with temperature units that determines the depth of the distribution. The exponential distribution and the corresponding thermal electron distribution in the

I. Abayev · A. Zaban
Department of Chemistry, Bar-Ilan University,
Ramat-Gan 52900, Israel

V. G. Kytin · A. A. Danilin
Department of Physics, Moscow Lomonosov State University,
119992, GSP-2 Moscow, Russia

G. Garcia-Belmonte · J. Bisquert (✉)
Departament de Ciències Experimentals, Universitat Jaume I,
Castellon 12080, Spain
e-mail: bisquert@uji.es

bandgap are shown in Fig. 1. This type of distribution was widely used for interpreting the features of electron transport [12–14] and interfacial charge transfer (recombination in dye solar cells) [15, 16]. The origin of such bandgap states and their spatial location in the nanoparticles were discussed in recent papers [17–19].

To obtain detailed information on electronic states in nanostructured TiO₂ permeated with aqueous electrolyte, we report in this study the results of the accurate determination of the electronic DOS of particles of different sizes as a function of temperature. Recently, we developed a method for extracting the DOS with a high accuracy from the results of electron charging in nanostructured films [20]. In this study, we describe the first systematic application of this method. The results suggest that nanometer confinement has a significant influence on the density of electronic states in TiO₂ nanoparticles with a mean diameter of 10 nm.

Experimental

Nanoporous TiO₂ (anatase) electrodes were prepared using three suspensions that differ by the nanocrystal size: 10, 20, and 30 nm mean diameters, as shown in Fig. 2. The three TiO₂ suspensions were prepared by the hydrolysis of

titanium(IV) isopropoxide (Aldrich, 99.9%, 50% volume in 2-propanol) in acetic acid (pH=2). After aging for 10–48 h, the organic remainders were evaporated at 82 °C followed by a hydrothermal treatment (in a titanium autoclave, Parr). The different crystal sizes were achieved by variations of the aging period, the autoclaving temperature, and the autoclaving duration as shown in Table 1. The TiO₂ suspensions were transformed to gels by sonication for 5 min, addition of Carbowax (polyethylene glycol compound), and moderate stirring overnight.

Conductive glass substrates (Libby Owens Ford, 13 Ω/sq. F-doped SnO₂) were cleaned with soap, rinsed with deionized water, and dried in a nitrogen stream. The TiO₂ slurry was spread over the substrate with a glass rod using adhesive tape as spacers. The films were fired at 450 °C for 30 min in air.

The electrochemical measurements were performed in a standard three-electrode cell, the TiO₂ film being the working electrode, a Pt wire the counter electrode, and an Ag/AgCl electrode as reference electrode (RE). The measurements were performed in a pH 1.8 HClO₄ aqueous solution containing 0.2 M LiClO₄, at defined temperatures in the range of 5–55 °C. The LiClO₄ was added to increase the electrolyte conductivity. This could be done also with HClO₄, which, however, is the acid used in this case that influences the pH. Therefore, we use the combination of HClO₄ and LiClO₄ to independently get the desired pH and conductivity. Because the voltammogram measurement is quite fast, intercalation effects are not expected. No correction is made for the small temperature dependence of the RE.

An Eco Chemie potentiostat (PG-30) was used to measure the current–voltage correlation. TEM (JEOL-JEM 100SX) and XRD (Bruker D8, CuK_α radiation) were used to determine the size and structure of the TiO₂ crystals. The thicknesses of the TiO₂ films were measured with SurfTest SV 500 profilometer (Mitutoyo).

Materials and methods

Electron charging as a function of film potential, $n(U)$ was determined by CV as described previously [20]. This method [5, 20] monitors the current injected in the film as the potential varies at a constant speed, $s=dU/dt$. The electronic current flowing into a unit volume is

$$j = -q \cdot \frac{dn}{dt} = -q \cdot \frac{dn}{dU} \cdot \frac{dU}{dt} = -q \cdot s \cdot \frac{dn}{dU} \quad (2)$$

As the voltage U becomes more negative, and assuming that the conduction band potential, E_c , is stationary, the Fermi level inside the TiO₂ nanostructure is displaced toward the conduction band, as indicated in Fig. 1.

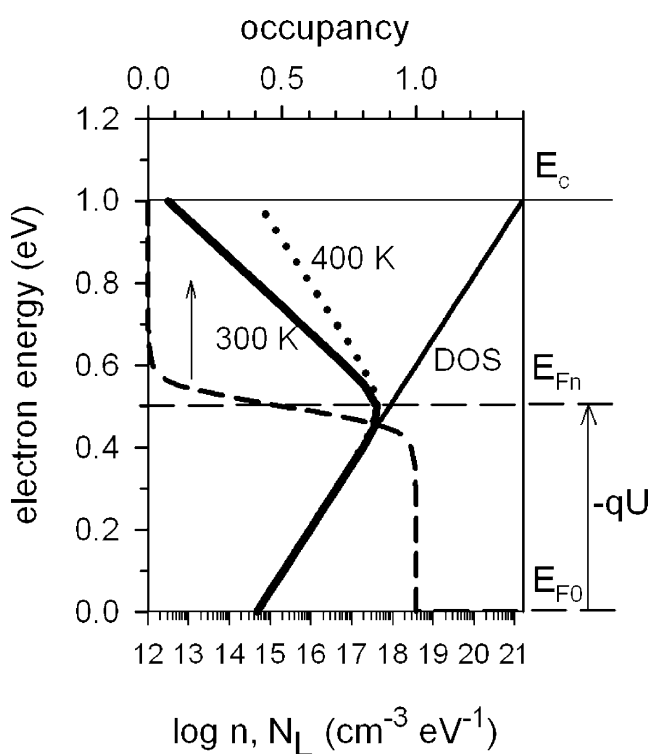
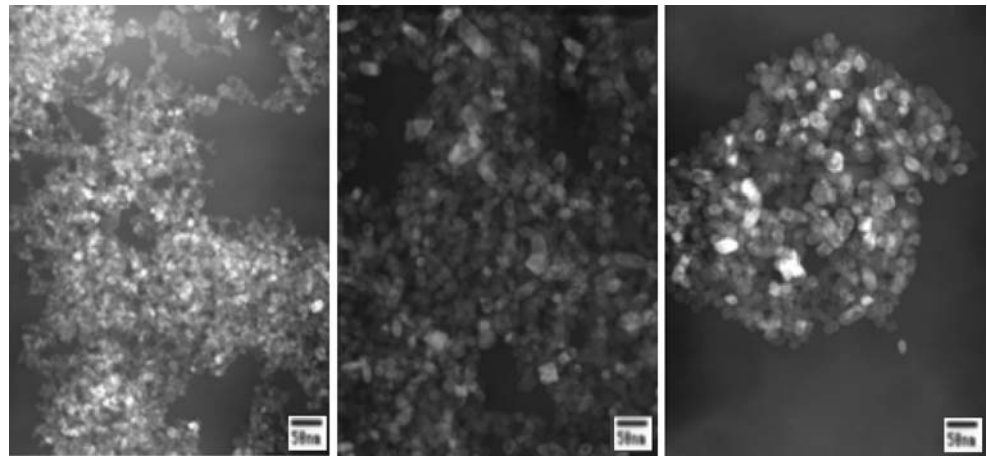


Fig. 1 Quantitative representation of the thermal occupation at temperature $T=300$ K (thick line) of an exponential DOS in the bandgap (thin line) with $T_0=800$ K and $N_L=10^{20}$ cm⁻³, as determined by the Fermi–Dirac distribution function (dashed line). The dotted line indicates the distribution of carriers at $T=400$ K

Fig. 2 TEM pictures of TiO₂ nanoparticles that are 10, 20, and 30 nm in diameter (from left to right). The bar below is 50-nm-wide



Let us consider the determination of the DOS, $g(E)$, from the measured quantity, dn/dU . The electron density at a certain potential is given by the expression

$$n(U) = \int_{-\infty}^{\infty} g(E) \cdot f\left(\frac{E - E_{Fn}}{k_B \cdot T}\right) dE \quad (3)$$

The following variable describes the distance of a certain energy level, E , to the Fermi level normalized to the thermal energy

$$x = \frac{E - E_{Fn}}{k_B \cdot T} \quad (4)$$

We can write Eq. 3 as

$$n(U) = k_B \cdot T \cdot \int_{-\infty}^{\infty} g(k_B \cdot T \cdot x + E_{Fn} - q \cdot U) f(x) dx \quad (5)$$

In Eq. 3, $f(x)$ is the distribution function. For localized states in semiconductors, coulomb repulsion prevents the occupation of the same localized state by two electrons with different spin orientations. Therefore, the distribution function of such states is often taken in the form of a modified Fermi–Dirac distribution function:

$$f(x) = \frac{1}{2} \cdot \left[1 + \frac{1}{2} e^x \right]^{-1} \quad (6)$$

Expression 6 accounts for the fact that only one half of states can be occupied in this situation.

The quantity of experimental interest is the derivative

$$\frac{dn}{dU} = -q \cdot k_B \cdot T \cdot \int_{-\infty}^{\infty} \frac{dg}{dE_{Fn}} \cdot f(x) dx \quad (7)$$

Performing an integration by parts, Eq. 7 takes the form

$$\frac{dn}{dU} = q \cdot \int_{-\infty}^{\infty} g(k_B \cdot T \cdot x + E_{Fn} - q \cdot U) \cdot \frac{df}{dx}(x) dx \quad (8)$$

It is observed in Eq. 8 that the measured dn/dU involves an integration of $g(E)$, so that a deconvolution procedure is needed to extract the DOS. One simple solution to this problem is to use the zero temperature limit of the distribution function. In this case, as $k_B T \rightarrow 0$ in Eq. 4, Eq. 6 becomes a step function:

$$\begin{aligned} f &= 1/2 & \text{if } E \leq E_F \\ &= 0 & \text{if } E > E_F \end{aligned} \quad (9)$$

Then the derivative df/dx becomes a Dirac- δ and Eq. 8 gives the simple result

$$g_0(E_{Fn} - q \cdot U) = -\frac{2}{q} \cdot \frac{dn}{dU} \quad (10)$$

The interpretation of Eq. 10 is that the extent of charging related to the perturbation dU corresponds to filling a slice of traps at the Fermi level. Most methods used so far in the determination of the DOS have applied the approximation in Eq. 10 [21]. However, Eq. 10 completely neglects the effect of the thermal spread of the distribution function in the region around the Fermi level. Therefore, some features of the true DOS can be hidden or invisible in the approximation of Eq. 10. Figure 3 shows as an example

Table 1 Preparation of nanocrystalline TiO₂ particles

Crystal diameter (nm)	Aging duration (h)	Autoclaving temp. (°C)	Autoclaving duration (h)
10	10	150	5
20	10	250	13
30	48	250	13

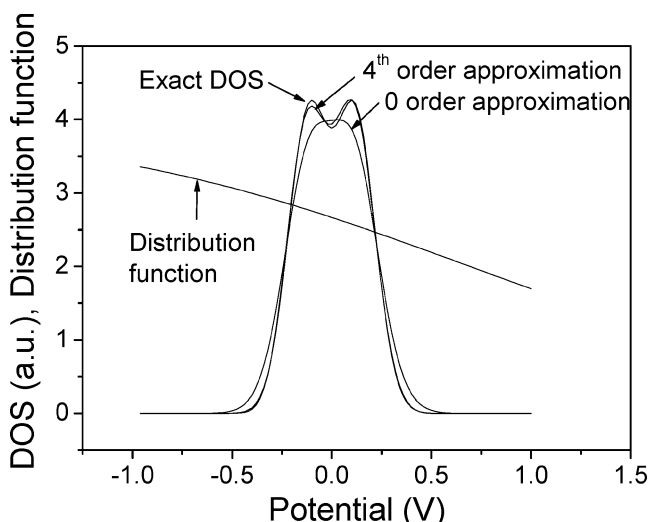


Fig. 3 Simulated DOS with a double Gaussian peak and Fermi–Dirac distribution function at finite T . The approximations (zero and fourth order) to the DOS determined from the dependence of number of occupied states on Fermi energy, as described in the text, are shown

the function $g_0(E_{Fn})$ calculated for a DOS consisting of two Gaussian peaks and the distribution function of Eq. 6. It is obvious that g_0 looks quite different from the DOS at finite temperature, although $k_B T$ is clearly less than the distance between peaks. Thus, the temperature broadening of the distribution function can lead to a significant error in the determination of the DOS.

A more accurate method for obtaining the DOS in Eq. 8 was developed [20] that takes into account the temperature dependence of the electron density. The method is based on a series expansion of g in Eq. 8 with respect to $k_B T$:

$$\frac{dn}{dU} = -q \cdot \left[g(E_{F0} - q \cdot U) \cdot f(-\infty) + \sum_{l=1}^{\infty} \alpha_l \cdot \frac{d^l g}{dU^l} \cdot \left(\frac{k_B \cdot T}{q} \right)^l \right] \tag{11}$$

where

$$\alpha_l = -\frac{(-1)^l}{l!} \cdot \int_{-\infty}^{\infty} x^l \cdot \frac{df}{dx} dx \tag{12}$$

An iteration procedure was applied to extract the DOS function from Eq. 11. First, the zero order approximation for DOS was taken in the form:

$$g_0(E_{F0} - q \cdot U) = -\frac{1}{q \cdot f(-\infty)} \cdot \frac{dn}{dU} \tag{13}$$

Then a first order correction δg_1 is found by substitution $g_0(E_{F0}-q \cdot U) + \delta g_1(E_{F0}-q \cdot U)$ in the first term in brackets of the right side of Eq. 11, and $g_0(E_{F0}-q \cdot U)$ in the rest of the expansion where only the term containing $k_B T$ has to be

taken for first order correction. Similarly, higher order corrections can be found and the expression for the DOS takes the form:

$$g(E_{F0} - q \cdot U) = -\frac{1}{q \cdot f(-\infty)} \cdot \left[\frac{dn}{dU} + \sum_{l=1}^{\infty} b_l \cdot \frac{d^{l+1} n}{dU^{l+1}} \cdot \left(\frac{k_B \cdot T}{q} \right)^l \right] \tag{14}$$

where

$$b_1 = -\frac{\alpha_1}{f(-\infty)}; \quad b_l = -\frac{1}{f(-\infty)} \cdot \left(\alpha_l + \sum_{m=1}^{l-1} b_m \cdot \alpha_{l-m} \right) \tag{15}$$

The series converges rapidly and provides very accurate results already at the fourth order of summations. As an example, the fourth approximation of the model DOS is presented in Fig. 3.

For the distribution function in Eq. 6, the coefficients in Eq. 15 have the values:

$$\begin{aligned} b_1 &= -0.6931471806 \\ b_2 &= -1.4047075599 \\ b_3 &= 1.084677302 \\ b_4 &= 0.4262037893 \end{aligned}$$

The application of Eq. 14 to the voltammetry data requires a determination of the higher order derivatives of $n(U)$. Because the experimental data contain noise, a certain smoothing is required to perform digital differentiation of higher orders. Derivatives were calculated digitally with a smoothing of the data (three triple 5 points procedure) applied before each differentiation. To reduce the amplification of noise in high order derivatives the data were smoothed by adjacent averaging procedure using ORIGIN 7.0 software once before each differentiation. The number of averaging points was taken equal to 7. For a number of points less than or equal to 4, the essential increase of noise in the fourth approximation of DOS was observed. For more than ten points of averaging a noticeable suppression of well reproducible features of the DOS took place.

Results and discussion

The measured CVs were nearly symmetric as shown in Fig. 4, ensuring a low level of electron transfer to the electrolyte [5]. The fourth order DOS calculated from the cathodic part of the voltammetric scans by means of Eq. 14

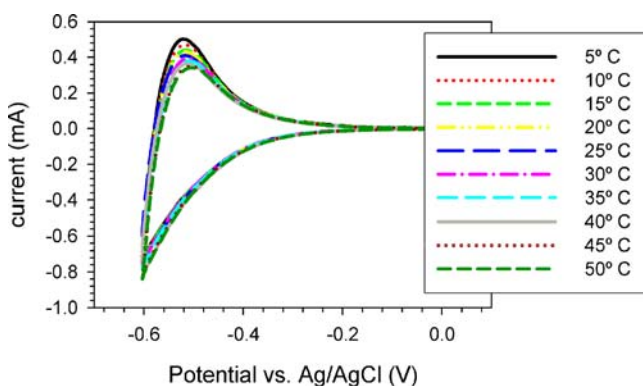


Fig. 4 Cyclic voltammograms of TiO₂ film formed by sintered nanoparticles with a diameter of 20 nm at different temperatures. The scan rate is 50 mV/s

is presented in Fig. 5. Due to the noise in the initial data it is safe to speak about features at potentials from -0.6 to -0.2 V. At higher potentials the data trends are strongly distorted by the noise smoothing procedure.

The DOS calculated for nanoporous TiO₂ consisting of 20- and 30-nm particles approaches very closely the exponential dependence indicated in Eq. 1, i.e., a straight line in log–lin representation. The DOS calculated for nanoporous TiO₂ consisting of 10-nm particles also exhibits the general tendency of an exponential distribution, but it shows an additional clear feature, consisting on a peak at -0.4 V (Ag/AgCl) over the general exponential tendency. This peak was found in past studies by several spectroelectrochemical techniques [21–23] and it was interpreted as a deep Ti⁴⁺ surface state with a distorted octahedral configuration [24, 25].

Another aspect of the results in Fig. 5 is the temperature dependence of the DOS [20].¹ It is observed that the slopes, for the 20- and 30-nm particles, are nearly temperature-independent, while the DOS for 10-nm nanoparticles is more strongly affected by the temperature changes. To analyze these trends in more detail, the linear part of all the data in Fig. 5 was fitted to a straight line, i.e., the DOS was treated as an exponential distribution, Eq. 1. The fitting parameter is the energy width of the exponential distribution, $\epsilon_0 = k_B T$. Therefore, a temperature dependence of the energy parameter $\epsilon_0(T)$ for the different films investigated was determined and is reported in Fig. 6. This procedure is an approximation but provides some valuable insight: For the 10-nm sample the energy parameter becomes larger at increasing temperature, changing from 80 to 100 meV. In contrast, for the larger particles the parameter ϵ_0 remains stable around 90 meV.

From these results, we obtain several observations. The small (10 nm) nanoparticles clearly show the peak of a

¹ In the previous paper, ref. 20, the labeling of the curves for 5 and 41 °C was mistakenly inverted in Fig. 4

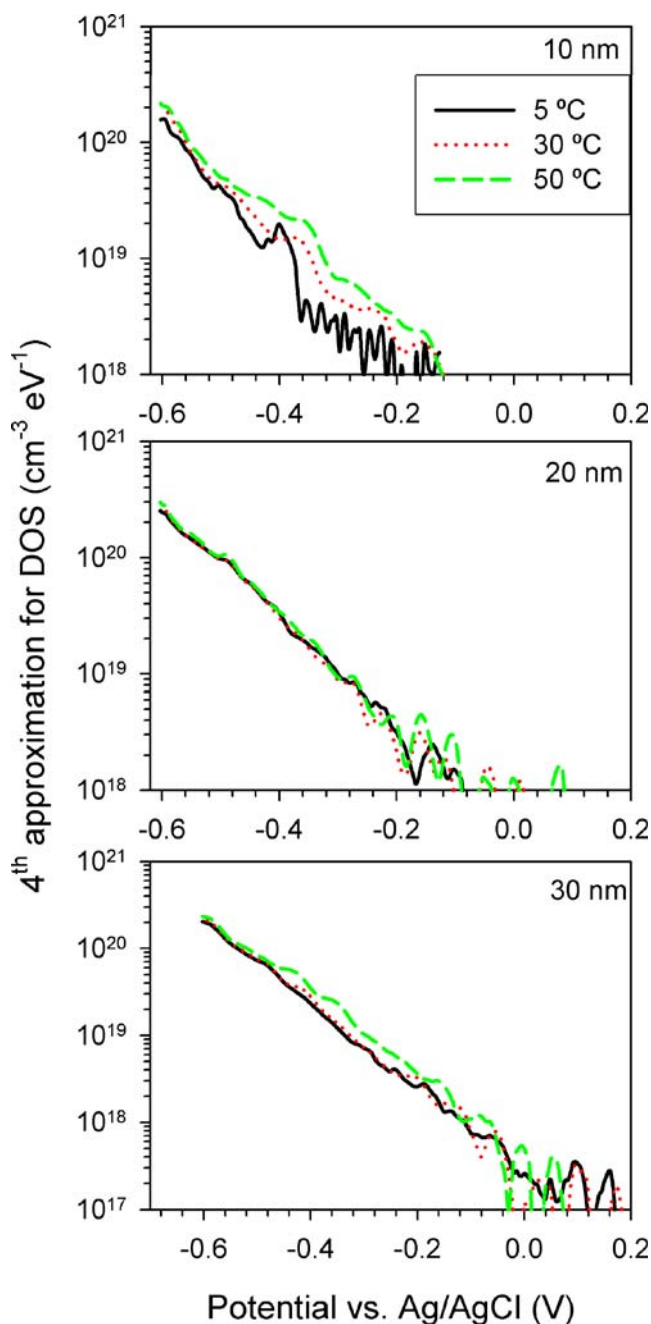


Fig. 5 Fourth order approximation of the DOS at finite temperatures in nanostructured TiO₂ films of different particle radii as indicated

surface state Ti⁴⁺/Ti³⁺, which becomes less significant for the larger nanoparticles. This first observation may be interpreted in terms of the decreasing relative importance of the surface in the larger particles.

A second observation relates to the fact that the exponential distribution is observed in the different nanoporous TiO₂ films studied, although with a different temperature dependence. For the larger, 20- to 30-nm particles, the exponential distribution is nearly temperature-independent, which is the standard behavior of band

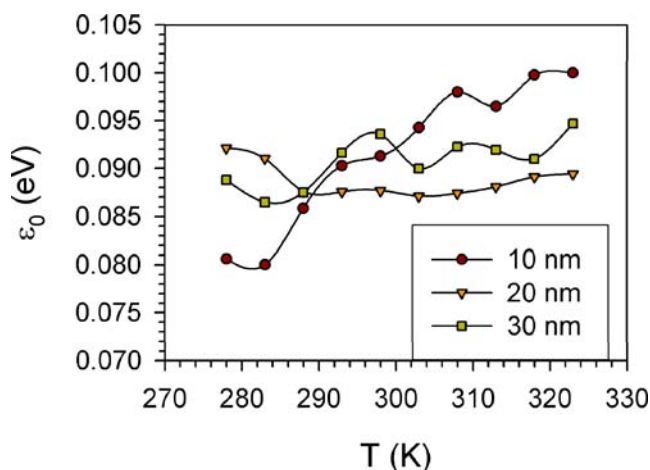


Fig. 6 Energy parameter $\varepsilon_0 = k_B T_0$ for an exponential DOS, resulting from a fit of the fourth order approximation of the DOS, shown in Fig. 5, to the distribution $g(E) = A \exp(E/\varepsilon_0)$, as a function of temperature in nanostructured TiO_2 films of different particle radii as indicated

tailing in bulk semiconductors, either impurity-induced or as a consequence of local coulombic interactions and dislocations of the bulk lattice [26].

For the small (10 nm) nanoparticles, a temperature variation of the tailing parameter of the exponential distribution is found (Fig. 6). We remark that a similar variation was reported recently from anomalous diffusion measurements by surface photovoltage transients [27, 28]. To explain this observation we tentatively propose a model of size confinement effect that was suggested in a recent publication [17]. The 10-nm nanoparticles can be considered as quantum dots where the electron wave functions experience a strong spatial confinement. The energy for addition of electrons to a quantum dot contains several contributions [29, 30]: the self-energy of the electron interacting with its image charge at the surface of the particle [31]; the electrostatic interactions, which are screened by the external medium; and the exchange energy. In particular, the dielectric mismatch at the boundary produces a strong influence on the discrete energy levels. It was shown [17] that the presence of impurities near the nanoparticle (10 nm radius) surface induces bandgap states, in which its distribution depends on the values of the dielectric constant of the particle and the surrounding medium, as a result of two combined effects. On the one hand, the coulomb potential (bare coulomb) generated by the impurity yields a penetration of electronic states into the gap, which is enhanced as the static dielectric constant of the quantum dot diminishes. In addition, if the internal (quantum dot) static dielectric constant is larger than the external (electrolyte) one, then the polarization-induced charge at the surface has the same sign as the impurity,

yielding an attractive interaction with the electron and increasing the binding energy. The interplay between coulomb terms (bare coulomb and surface polarization), in addition to the nanometer confinement, is responsible for the band tailing [17]. This effect is due to the nanometer size and appears in addition to the impurity-induced tailing in bulk semiconductors that was mentioned above [26], which is expected to be temperature-independent.

The experimental effect observed for small size particles may be explained by the temperature dependence of TiO_2 permittivity [32]. As the temperature is raised up, TiO_2 dielectric constant decreases, enhancing bare Coulombic terms in detriment of surface polarization charge. As a combined result, an increment in the DOS width parameter is produced [17]. As the particle size enlarges (20- and 30-nm particles) the confinement effect due to the dielectrically mismatched surface becomes less pronounced. Hence, bandtailing in these larger particles becomes temperature-independent as in bulk semiconductors.

Another explanation for the change of localized states distribution with temperature was provided [33] in terms of the random temporal fluctuations of the localized state energies. Such fluctuations mainly affect the deeply lying states, which have a slow release dynamics, and this model may explain the broadening of the $\text{Ti}^{4+}/\text{Ti}^{3+}$ peak with temperature that is observed in Fig. 5 for the 10-nm particles.

Conclusions

The density of electronic states in TiO_2 nanoparticles of 10 nm mean size is strongly affected by temperature variation while for particles with mean sizes of 20 and 30 nm the DOS is much closer to an exponential distribution, and is much less sensitive to temperature variations. Tentatively, the DOS for small (10 nm) nanoparticles can be ascribed to the confinement effect due to dielectric mismatch, while in larger particles this effect is minor and the exponential distribution is caused by of local coulombic interactions and dislocations of the bulk lattice.

Acknowledgement The work was supported by Ministerio de Educación y Ciencia of Spain under project MAT2004-05168.

References

1. Garcia-Belmonte G, Kytin V, Dittrich T, Bisquert J (2003) *J Appl Phys* 94:5261
2. Cinnsealach R, Boschloo G, Rao SN, Fitzmaurice D (1999) *Sol Energy Mater Sol Cells* 57:107
3. Garcia-Cañadas J, Fabregat-Santiago F, Porqueras I, Person C, Bisquert J, Garcia-Belmonte G (2004) *Solid State Ionics* 175:521

4. O'Regan B, Grätzel M (1991) *Nature* 353:737
5. Fabregat-Santiago F, Mora-Seró I, Garcia-Belmonte G, Bisquert J (2003) *J Phys Chem B* 107:758
6. Fabregat-Santiago F, Bisquert J, Garcia-Belmonte G, Boschloo G, Hagfeldt A (2005) *Sol Energy Mater Sol Cells* 87:117
7. Peter LM, Duffy NW, Wang RL, Wijayantha KGU (2002) *J Electroanal Chem* 127:524–525
8. Boschloo G, Hagfeldt A (2005) *J Phys Chem B* 109:12093
9. Palomares E, Clifford JN, Haque SA, Lutz T, Durrant JR (2003) *J Am Chem Soc* 125:475
10. Agrell HG, Boschloo G, Hagfeldt A (2004) *J Phys Chem B* 108:12388
11. Bisquert J (2003) *Phys Chem Chem Phys* 5:5360
12. Nelson J (1999) *Phys Rev B* 59:15374
13. van de Lagemaat J, Frank AJ (2000) *J Phys Chem B* 104:4292
14. van de Lagemaat J, Frank AJ (2001) *J Phys Chem B* 105:11194
15. Bisquert J, Zaban A, Salvador P (2002) *J Phys Chem B* 106:8774
16. Bisquert J, Zaban A, Greenshtein M, Mora-Seró I (2004) *J Am Chem Soc* 126:13550
17. Movilla JL, Garcia-Belmonte G, Bisquert J, Planelles J (2005) *Phys Rev B* 72:153313
18. Kopidakis N, Neale NR, Zhu K, van de Lagemaat J, Frank AJ (2005) *Appl Phys Lett* 87:202106
19. Olson CL, Nelson J, Islam MS (2006) *J Phys Chem B* 110:9995
20. Kytin VG, Bisquert J, Abayev I, Zaban A (2004) *Phys Rev B* 70:193304
21. Wang H, He J, Boschloo G, Lindström H, Hagfeldt A, Lindquist S (2001) *J Phys Chem B* 105:2529
22. Redmond G, Fitzmaurice D, Grätzel M (1993) *J Phys Chem* 97:6951
23. Boschloo GK, Goossens A (1996) *J Phys Chem* 100:19489
24. Cao F, Oskam G, Searson PC, Stipkala JM, Heimer TA, Farzad F, Meyer GJ (1995) *J Phys Chem* 99:11974
25. de Jongh PE, Vanmaekelbergh D (1997) *J Phys Chem B* 101:2716
26. Pankove JI (1971) *Optical Processes in Semiconductors*. Prentice-Hall, Englewood Cliffs, NJ
27. Dittrich T, Mora-Seró I, Garcia-Belmonte G, Bisquert J (2006) *Phys Rev B* 73:045407
28. Mora-Seró I, Anta JA, Garcia-Belmonte G, Dittrich T, Bisquert J (2006) *J Photochem Photobiol A Chem* 182:280
29. Franceschetti A, Williamson A, Zunger A (2000) *J Phys Chem B* 104:3398
30. Franceschetti A, Zunger A (2000) *Appl Phys Lett* 76:1731
31. Brus LE (1984) *J Chem Phys* 80:4403
32. Parker RA (1964) *Phys Rev* 124:1719
33. Arkhipov VI, Adriaenssens GJ (1998) *J Non-Cryst Solids* 166:227–230